Available online at www.sciencedirect.com

ScienceDirect

Ceramics International 39 (2013) 8841–8846

CERAMICS INTERNATIONAL

www.elsevier.com/locate/ceramint

Preparation and characterization of $LnMgAl_{11}O_{19}$ (Ln = La, Nd, Gd) ceramic powders

Ren-Xian Zhu, Zhan-Guo Liu, Jia-Hu Ouyang*, Yu Zhou

Institute for Advanced Ceramics, School of Materials Science and Engineering, Harbin Institute of Technology, 92 West Da-Zhi Street, Harbin 150001, China

Received 1 April 2013; received in revised form 22 April 2013; accepted 22 April 2013
Available online 27 April 2013

Abstract

Lanthanide hexaaluminate powders of $LaMgAl_{11}O_{19}$ (LMA), $NdMgAl_{11}O_{19}$ (NMA) and $GdMgAl_{11}O_{19}$ (GMA) were synthesized via the solid state reaction or sol–gel and calcination method. The LMA and NMA powders synthesized by the sol–gel and calcination method at 1600 °C for 8 h exhibit a single hexaaluminate phase with magnetoplumbite structure; however, the GMA powder synthesized by the sol–gel and calcination method at 1600 °C for 8 h contains both a hexaaluminate phase and a small amount of second phase $GdAlO_3$ with a perovskite structure. The powders synthesized by the solid state reaction method at 1500 °C for 4 h have a small particle size of 1–3 μm, and a large specific surface area and a good uniformity. The powders synthesized by the sol–gel and calcination method at 1600 °C for 8 h have a particle size of 5–20 μm, and exhibit to a certain extent agglomeration.

Keywords: Rare-earth hexaaluminate; Solid state reaction; Sol–gel method

1. Introduction

With the development of high thrust-weight ratio advanced turbine engines, one of the important issues is to enhance the operating temperature and efficiency of hot-section components. In recent years, thermal barrier coatings (TBCs) have been widely used to protect hot-section metal components in advanced gas-turbine (aircraft and power generation) and diesel engines [1–6]. Thermal barrier coatings system is generally composed of a porous and insulating ceramic oxide top layer, a thermally grown aluminum-rich oxide layer (TGO), which provides oxidation and hot corrosion protection, and an underlying bond layer which is used to form the TGO layer [7–9]. 6–8 wt% yttria-stabilized zirconia (YSZ) thermal barrier coatings, which are generally produced by plasma spraying or electron beam physical vapor deposition, are widely used to provide thermal insulation for hot section components of superalloys [10–12]. However, 6–8 wt% YSZ is limited to applications below 1200 °C due to its limited sintering resistance and phase stability during long-term service. 6–8 wt% YSZ TBCs system is currently capable of reducing metal temperature by about 150 °C, whereas potential benefits are estimated to be greater than 200 °C. In order to further increase the operating efficiency, it urgently needs to develop new thermal barrier oxides with significantly low thermal conductivity, high thermal expansion coefficient and high phase stability at elevated temperatures [3,13,14]. Lanthanide magnesium hexaaluminate ($LnMgAl_{11}O_{19}$, Ln=lanthanide) ceramics are a kind of important candidate materials for a variety of applications as combustion catalyst supports, active elements of solid-state lasers and ceramic thermal barrier coatings due to their good thermal stability, thermal insulating and optical properties. Chen et al. developed a plasma sprayed $LaMgAl_{11}O_{19}$/YSZ thermal barrier coating, and found that the platelet-like LMA grains improved the sintering resistance of composite coatings [15]. $LaMgAl_{11}O_{19}$–$Yb_3Al_5O_{12}$ composites prepared by pressureless sintering have a thermal conductivity in the range of 2.6–3.9 $W\,m^{-1}\,K^{-1}$ from room temperature to 1200 °C [16]. The quality of the starting powders has an important influence on the performance of hexaaluminate coatings. In the present work, $LaMgAl_{11}O_{19}$ (LMA), $NdMgAl_{11}O_{19}$ (NMA) and $GdMgAl_{11}O_{19}$ (GMA) powders were synthesized by the solid state reaction or sol–gel and calcination method, and microstructure of synthesized powders were analyzed.

*Corresponding author. Tel./fax: +86 451 86414291.
E-mail address: ouyangjh@hit.edu.cn (J.-H. Ouyang).

0272-8842/$ - see front matter © 2013 Elsevier Ltd and Techna Group S.r.l. All rights reserved.
http://dx.doi.org/10.1016/j.ceramint.2013.04.073

2. Experimental procedures

2.1. Preparation of $LnMgAl_{11}O_{19}$ powders by the solid state reaction method

$Al(OH)_3$, Ln_2O_3 (Ln=La, Nd, Gd) and $4MgCO_3 \cdot Mg(OH)_2 \cdot 5H_2O$ powders were used as raw materials. The raw materials were mixed in appropriate molar ratio to form $LnMgAl_{11}O_{19}$ powders by the solid state reaction method. Taking the $LaMgAl_{11}O_{19}$ as an example, the molar ratio of respective raw materials of $n_1(La_2O_3):n_2(4MgCO_3 \cdot Mg(OH)_2 \cdot 5H_2O):n_3(Al(OH)_3)$ is 1:0.4:22. The rare earth oxides were calcined at 900 °C for 2 h in air before weighing as they may be hygroscopic. An appropriate amount of ethanol is added into the mixture to form a powder pasty. The powder mixture was ball-milled for 24 h and were then dried at 130 °C in air, and finally calcined in an air furnace at 1500 °C for 4 h to form hexaaluminate powders.

2.2. Preparation of $LnMgAl_{11}O_{19}$ powders by the sol–gel and calcination method

$LnMgAl_{11}O_{19}$ powder precursors were synthesized by the sol–gel method. Ln_2O_3 (Ln=La, Nd, Gd), $Al(NO_3)_3 \cdot 9H_2O$ and $Mg(NO_3) \cdot 6H_2O$ powders were used as raw materials, while citric acid ($C_6H_8O_7 \cdot H_2O$) was used as a chelating agent. For each composition, rare earth oxides were firstly calcined at 900 °C for 2 h, and were then accurately weighed and dissolved in dilute nitric acid. The pH value of the solution was adjusted to between 5 and 6 using ammonia. $Al(NO_3)_3 \cdot 9H_2O$ and $Mg(NO_3) \cdot 6H_2O$ powders were added into the solution after rare earth oxides were completely dissolved. After stirring, the mixture was put into a beaker for ultrasonic dissolving, and was then filtered. The molar ratio of citric acid ($C_6H_8O_7 \cdot H_2O$) to metallic cations was set to be 1.2:1. Appropriate amount of distilled water was added to form a solution of 0.1 mol L^{-1} Ln^{3+}. The solution was stirred at room temperature for 24 h, and was firstly held at 90 °C for 100 h, and then at 120 °C for 24 h to generate loose pupil xerogel precipitates. Finally, these xerogels were calcined at 1600 °C for 8 h in an air furnace to obtain final products of $LnMgAl_{11}O_{19}$ (Ln=La, Nd, Gd) powders.

2.3. Characterization

Fourier transform infrared spectroscopy of the synthesized xerogel powders was performed using a Nicolet Magna-IR 560E. S.P. spectrometer. Thermogravimetry (TG) and differential thermal analysis (DTA) of the synthesized xerogels were carried out using a simultaneous thermal analysis apparatus (Netzsch STA 449C, Germany) with a heating rate of 10 °C min^{-1} and an air flow of 30 mL min^{-1} in corundum crucibles from room temperature to 1450 °C. X-ray diffraction analysis was performed with a Rigaku D/Max 2200VPC X-ray diffractometer using Cu Kα-radiation and graphite monochromator with a voltage of 40 kV and a current of 30 mA, and a scanning rate of 4°/min. The particle size distribution of $LnMgAl_{11}O_{19}$ (Ln=La, Nd, Gd) ceramic powders was measured with a LA-920 laser scattering analyzer, and the relative refractive index used in this work is 1.7. Dilute suspension of ceramic powders in ethanol was taken onto aluminum foils and coated with thin carbon coating for scanning electron microscopy (FEI Quanta 200F, the Netherlands).

3. Results and discussion

3.1. FT-IR absorption spectroscopy

Fig. 1 shows the Fourier transform infrared absorption spectrum of the synthesized $LaMgAl_{11}O_{19}$ xerogels. The absorption peak at 3410 cm^{-1} is due to the stretching vibration absorption of citrate O–H, while two weak absorption peaks at 2350 and 2560 cm^{-1} result from the Fermi resonance created by the baseband of the O–H stretching vibration and the combined frequency combination frequency of the bending vibrations of the C–O–H and the stretching vibration of the C–O. The absorption peak at 1600 cm^{-1} is caused by the asymmetric stretching vibration of the citrate –COO, while the peak at 1080 cm^{-1} is due to the vibration absorption of the C–O and the C–O in citrate is also close to the big π bond. The broadened absorption peak near the 500 cm^{-1} is due to the stretching vibration of the M–O bond of citrate, while the weak peaks at 600 to 800 cm^{-1} and the strong peak at 1350 cm^{-1} are due to the stretching vibrations and absorption of the $-NO_3$. There are several weak peaks at about 1500 cm^{-1}, which may depend upon the stretching absorption of the antisymmetric-NO_3. The structural features of these molecules confirm that the xerogels are composed of citric acid, citrate and a small amount of nitrate.

3.2. Thermogravimetry and differential thermal analysis

Thermal decomposition behavior of the xerogels in air is shown in Fig. 2. As clearly revealed from TG–DTA curves from room temperature to about 300 °C, TG curve shows a slow mass loss, while the corresponding DTA curve has several small endothermic valleys due to the loss of free water or the endothermic of the

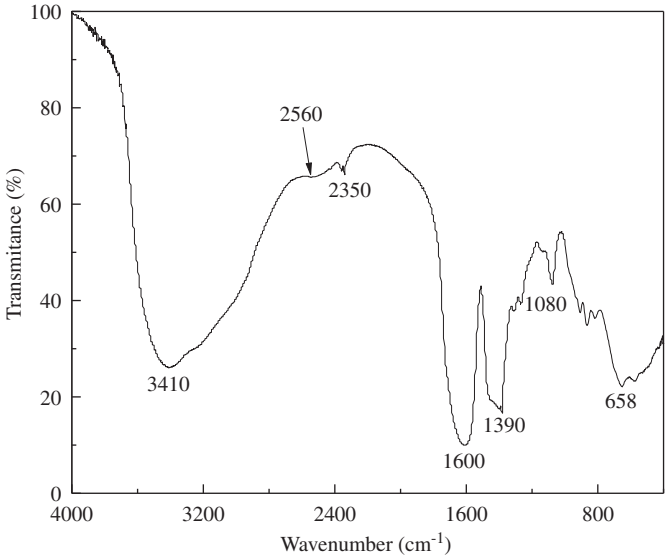

Fig. 1. FT-IR spectrum of $LaMgAl_{11}O_{19}$ xerogels.

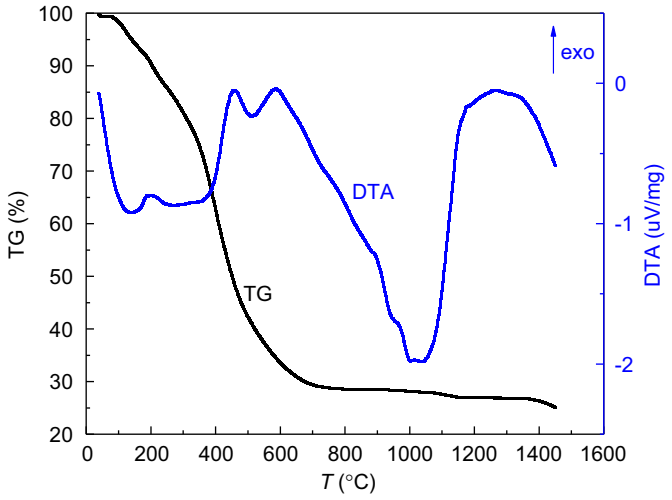

Fig. 2. TG–DTA curves of $LaMgAl_{11}O_{19}$ xerogels.

adsorbed water in the citric acid xerogels. The xerogels are easy to absorb water in air due to the honeycomb porous organizational structure. From 300 to 600 °C, the xerogels rapidly lose mass. From the DTA curve, two exothermic peaks near 440 and 600 °C are caused by the citrate decomposition and the combustion heat release. Thermogravimetry analysis shows major weight loss up to 600 °C. The weight loss is found to be negligible above 800 °C. A small exothermic peak in the DTA curve between 900 and 950 °C is due to an intermediate phase crystallization exotherm, and the strong peak between 1100 and 1300 °C is due to the chemical reaction in the xerogels and the formation of $LaMgAl_{11}O_{19}$ powders.

3.3. X-ray diffraction analysis

Fig. 3 shows the XRD patterns of the $LnMgAl_{11}O_{19}$ products synthesized by different methods. From Fig. 3(a–c),

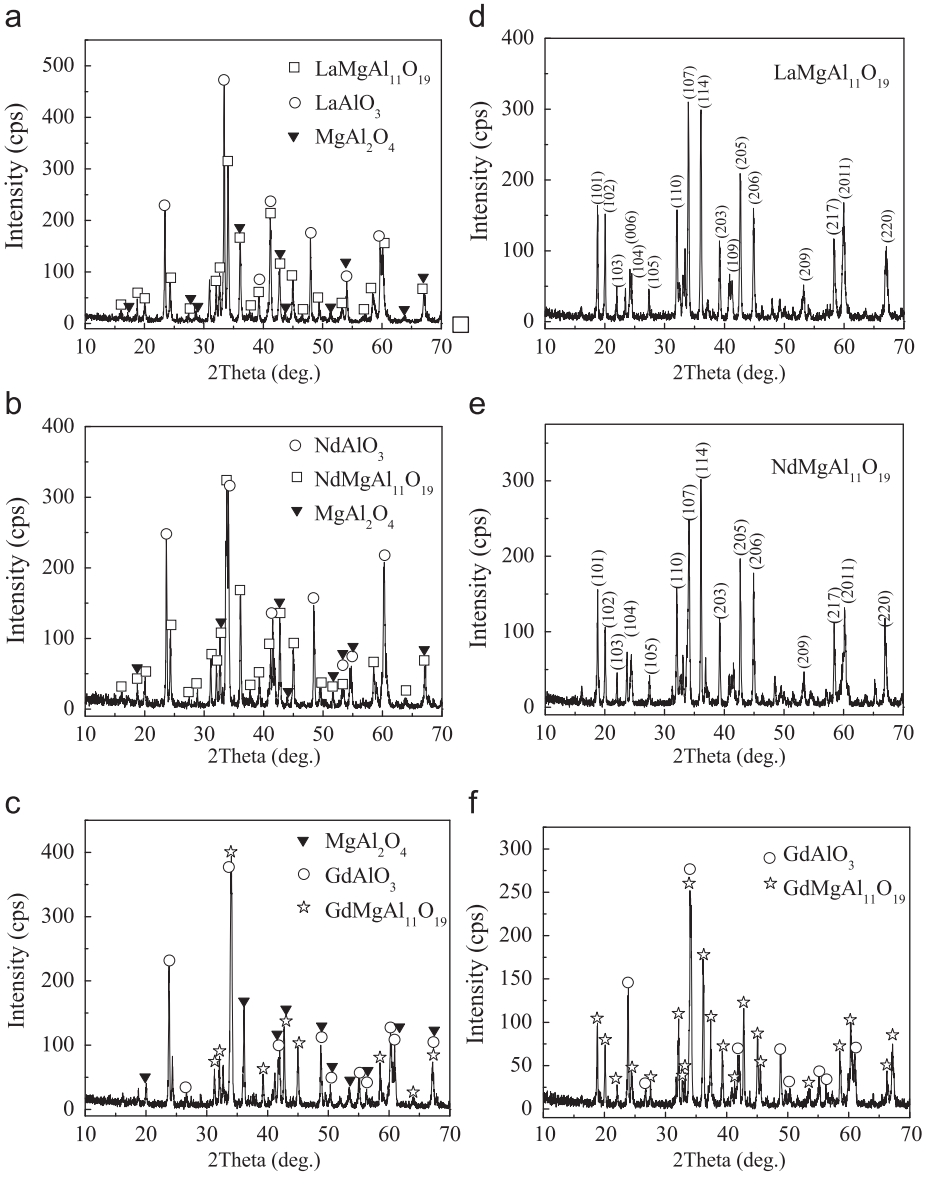

Fig. 3. XRD patterns of different $LnMgAl_{11}O_{19}$ products synthesized by different methods: (a) LMA, (b) NMA, (c) GMA synthesized by the solid state reaction method at 1500 °C for 4 h, (d) LMA, (e) NMA and (f) GMA synthesized by the sol–gel and calcination method at 1600 °C for 8 h.

the LMA, NMA and GMA products synthesized by the solid state reaction method at 1500 °C for 4 h exhibit a single hexaaluminate phase with a magnetoplumbite structure, and a small amount of second phase $LnAlO_3$ (Ln = La, Nd, Gd) with a perovskite structure. In addition, a very small amount of $MgAl_2O_4$ with a spinel structure is also found in Fig. 3(a–c). XRD patterns of the $LnMgAl_{11}O_{19}$ products synthesized by the sol–gel and calcination method at 1600 °C for 8 h are shown in Fig. 3(d–f). The synthesized LMA and NMA products exhibit a single hexaaluminate phase with magnetoplumbite structure; however, the GMA product contains both a hexaaluminate phase and a very small amount of second phase $GdAlO_3$ with a perovskite structure.

3.4. Particle size distribution of $LnMgAl_{11}O_{19}$ products

Fig. 4 shows the particle size distribution of the $NdMgAl_{11}O_{19}$ product synthesized by different methods, and the particle size distribution measured by a laser scattering technique is shown in Table 1. The product (A) prepared by the solid state reaction method at 1500 °C for 4 h has a small particle size, and a large specific surface area and a good uniformity. However, the product (B) prepared by the sol–gel method and one-step calcination method at 1600 °C for 8 h has a large particle size and a poor uniformity. The product (C) prepared by the sol–gel and two-step calcination method at 1000 °C for 4 h and 1100 °C for 6 h also exhibits a large particle size and a poor uniformity due to low crystallinity.

3.5. SEM observations

Fig. 5 shows SEM photographs of different $LnMgAl_{11}O_{19}$ products prepared by the solid state reaction or sol–gel and calcination method. The crystal growth of $LnMgAl_{11}O_{19}$ products is clearly anisotropic, while the crystal morphology is tablet-shaped and exhibits to a certain extent agglomeration. The powders prepared by the sol–gel and calcination method have a relatively smooth surface and a particle size of about 5–20 μm due to high calcination temperature and long holding time. However, the powders prepared by the solid-state

Table1
Particle size distribution of $NdMgAl_{11}O_{19}$ powders synthesized by different processing conditions.

Processing conditions	A	B	C
Specific surface area ($\times 10^3$ cm^2/cm^3)	42.2	13.8	8.24
Median particle size (μm)	1.62	5.97	14.7
Mean particle size (μm)	1.76	7.33	25.2
Variance (μm^2)	0.659	30.7	852
S.D. (μm)	0.812	5.54	29.2
CV	46.1	75.6	116
Mode particle size (μm)	1.84	5.52	14.2

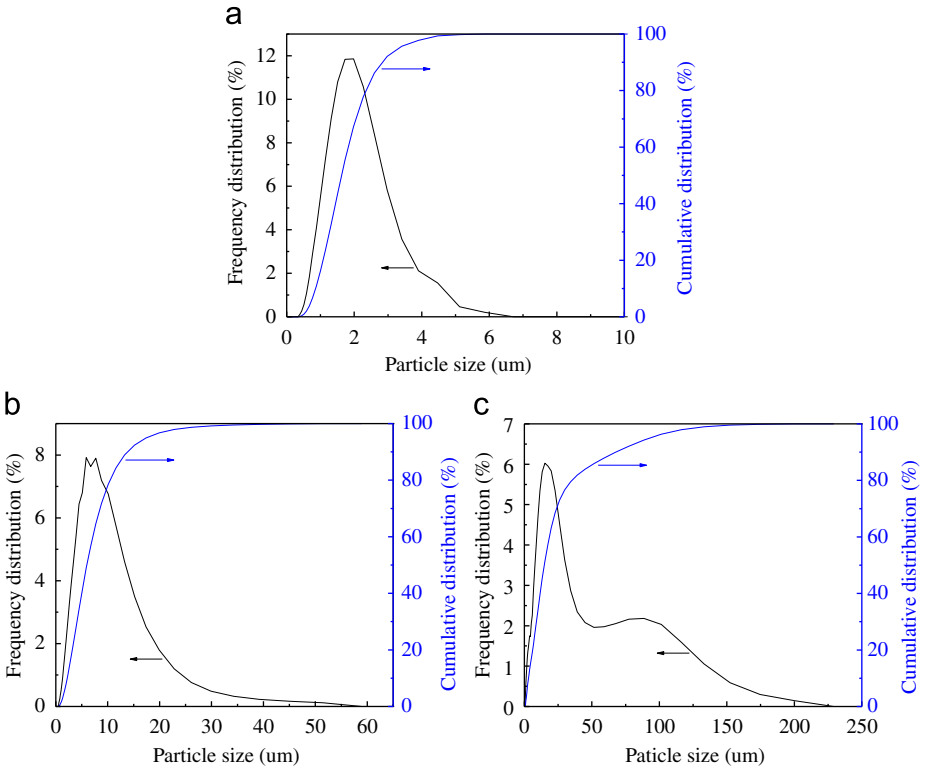

Fig. 4. Particle size distribution of $NdMgAl_{11}O_{19}$ powders synthesized by different processing conditions: (a) solid-state reaction method at 1500 °C for 4 h, (b) sol–gel and calcination method at 1600 °C for 8 h and (c) sol–gel and two-step calcination method at 1000 °C for 4 h and at 1100 °C for 6 h, respectively.

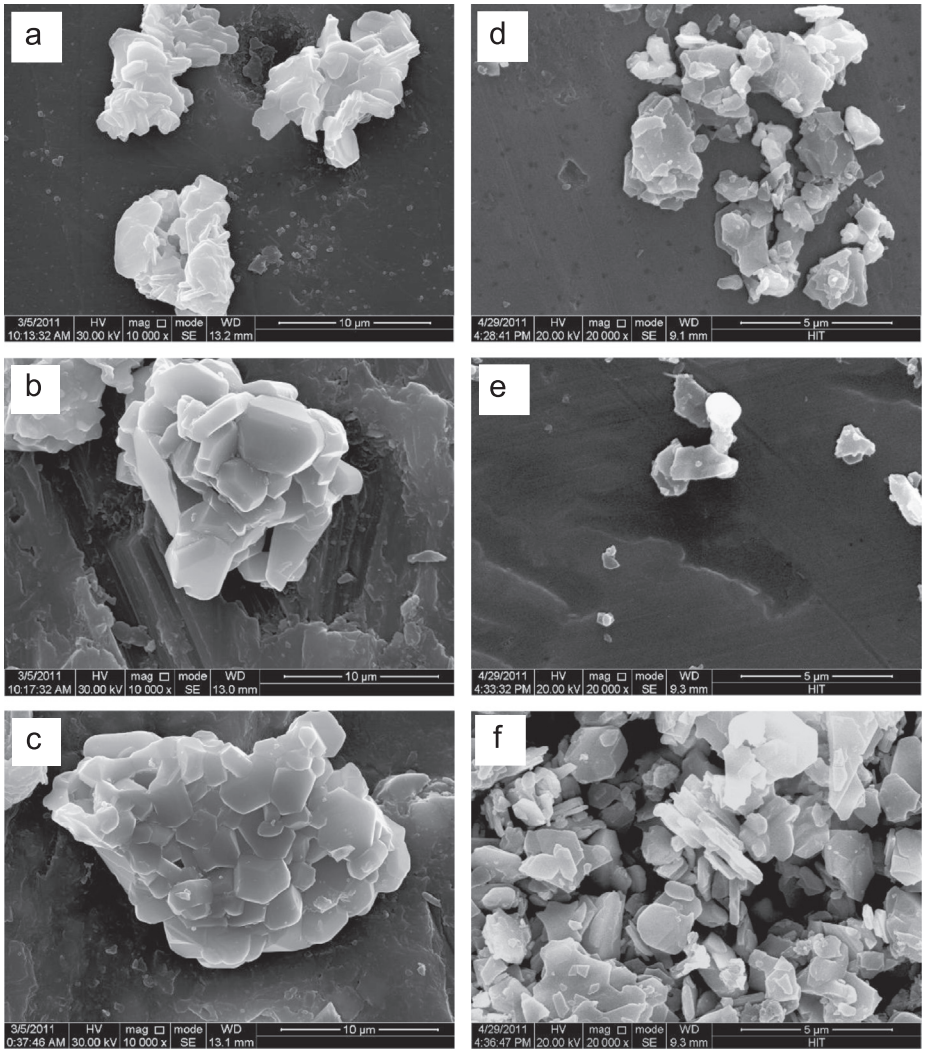

Fig. 5. SEM morphologies of different $LnMgAl_{11}O_{19}$ products synthesized by different methods: (a) LMA, (b) NMA and (c) GMA synthesized by the sol–gel and calcination method at 1600 °C for 8 h; (d) LMA, (e) NMA and (f) GMA synthesized by the solid state reaction method at 1500 °C for 4 h.

reaction method exhibit a good dispersion and has a particle size of about 1–3 μm due to low calcination temperature. $LaMgAl_{11}O_{19}$ with a tablet morphology exhibits a magnetoplumbite structure. In the superlattice structure of the spinel layer, the LaO_3 layer exhibits a crystallographic mirror, which is followed by a four-aluminum spinel layer. In this case, the aluminum spinel layer is separated by a symmetrical mirror. In the LaO_3 layer, La^{3+} cationsoccupy the sites of oxygen anions in the hexagonal closely packed structure of the anions, the ionic diffusion is strongly suppressed, and therefore, the crystal with a layered structure grows slowly along the *c*-axis direction perpendicular to the mirror.

4. Conclusions

(1) Lanthanide hexaaluminate powders of $LaMgAl_{11}O_{19}$, $NdMgAl_{11}O_{19}$ and $GdMgAl_{11}O_{19}$ were synthesized via the solid state reaction or sol–gel and calcination method.
(2) The $LaMgAl_{11}O_{19}$ and $NdMgAl_{11}O_{19}$ powders synthesized by the sol–gel and calcination method at 1600 °C for 8 h exhibit a single hexaaluminate phase with the magnetoplumbite structure; however, the $GdMgAl_{11}O_{19}$ powder synthesized by the sol–gel and calcination method at 1600 °C for 8 h contains a hexaaluminate phase and a small amount of second phase $GdAlO_3$ with a perovskite structure.
(3) The powders synthesized by the solid state reaction method at 1500 °C for 4 h have a small particle size of 1–3 μm, and a large specific surface area and a good uniformity. The powders synthesized by the sol–gel and calcination method at 1600 °C for 8 h have a particle size of 5–20 μm, and exhibit to a certain extent agglomeration.

Acknowledgments

This work was financially supported by the National Natural Science Foundation of China (NSFC, Grant nos. 51002038 and 51021002), and the Fundamental Research Funds for the Central Universities (Grant no. HIT.BRET1.2010006).

References

[1] R.A. Miller, Current status of thermal barrier coatings–an overview, Surface and Coatings Technology 30 (1987) 1–11.

[2] A.G. Evans, D.R. Mumm, J.W. Hutchinson, G.H. Meier, F.S. Pettit, Mechanisms controlling the durability of thermal barrier coatings, Progress in Materials Science 46 (2001) 505–553.

[3] N.P. Padture, M. Gell, E.H. Jordan, Thermal barrier coatings for gas-turbine engine applications, Science 296 (2002) 280–284.

[4] N.P. Bansal, D.M. Zhu, Thermal properties of oxides with magneto-plumbite structure for advanced thermal barrier coatings, Surface and Coatings Technology 202 (2008) 2698–2703.

[5] J.F. Zhang, X.H. Zhong, Y.L. Cheng, Y. Wang, Z.H. Xu, X.L. Chen, H.M. Ma, Y. Zhao, X.Q. Cao, Thermal-shock resistance of $LnMgAl_{11}O_{19}$ (Ln=La, Nd, Sm, Gd) with magnetoplumbite structure, Journal of Alloys and Compounds 482 (2009) 376–381.

[6] Z.-G. Liu, J.-H. Ouyang, Y. Zhou, S. Li, High-temperature hot corrosion behavior of gadolinium zirconate by vanadium pentoxide and sodium sulfate in air, Journal of the European Ceramic Society 30 (2010) 2707–2713.

[7] D.R. Clarke, C.G. Levi, Materials design for the next generation thermal barrier coatings, Annual Review of Materials Science 33 (2003) 383–417.

[8] A.G. Evans, D.R. Clarke, C.G. Levi, The influence of oxides on the performance of advanced gas turbines, Journal of the European Ceramic Society 28 (2008) 1405–1419.

[9] Z. Negahdari, M. Willert-Porada, F. Scherm, Thermal properties of homogenous lanthanum hexaaluminate/alumina composite ceramics, Journal of the European Ceramic Society 30 (2010) 3103–3109.

[10] R. Vassen, X.Q. Cao, F. Tietz, D. Basu, D. Stoever, Zirconates as new materials for thermal barrier coatings, Journal of the American Ceramic Society 83 (2000) 2023–2028.

[11] M.J. Pomeroy, Coatings for gas turbine materials and long term stability issues, Materials and Design 26 (2005) 223–231.

[12] M. Belmonte, Advanced ceramic materials for high temperature applications, Advanced Engineering Materials 8 (2006) 693–703.

[13] Z.-G. Liu, J.-H. Ouyang, Y. Zhou, J. Li, X.-L. Xia, $(Ln_{0.9}Gd_{0.05}Yb_{0.05})_2Zr_2O_7$ (Ln=Sm, Nd) ceramics with pyrochlore structure as thermal barrier oxides, Advanced Engineering Materials 10 (2008) 754–758.

[14] Z.-G. Liu, J.-H. Ouyang, B.-H. Wang, Y. Zhou, J. Li, Thermal expansion and thermal conductivity of $Sm_xZr_{1-x}O_{2-x/2}$ ($0.1 \le x \le 0.5$) ceramics, Ceramics International 35 (2009) 791–796.

[15] X.L. Chen, L.J. Gu, B.L. Zou, Y. Wang, X.Q. Cao, New functionally graded thermal barrier coating system based on $LaMgAl_{11}O_{19}$/YSZ prepared by air plasma spraying, Surface and Coatings Technology 206 (2011) 2265–2274.

[16] Y.-H. Wang, Z.-G. Liu, J.-H. Ouyang, Preparation and thermophysical properties of $LaMgAl_{11}O_{19}$–$Yb_3Al_5O_{12}$ ceramic composites, Ceramics International 37 (2011) 2489–2493.